RESEARCH ARTICLE

WILEY

Investigations of polygonal patterned ground in continuous Antarctic permafrost by means of ground penetrating radar and electrical resistivity tomography: Some unexpected correlations

Emanuele Forte[1] | Hugh M. French[2] | Rossana Raffi[3] | Ilaria Santin[1] | Mauro Guglielmin[4]

[1]Department of Mathematics and Geosciences, University of Trieste, Trieste, Italy

[2]Passed away. Department of Geography and Earth Sciences, University of Ottawa, Ottawa, Ontario, Canada

[3]Department of Earth Sciences, University La Sapienza, Rome, Italy

[4]Department of Theoretical and Applied Sciences, Insubria University, Varese, Italy

Correspondence
Emanuele Forte, Department of Mathematics and Geosciences, University of Trieste, Trieste, Italy.
Email: eforte@units.it

Funding information
PNRA, Grant/Award Numbers: 2013/AZ1.05, 18_00288-D, 18_00186-E

Abstract

The results of a combined geophysical and geomorphological investigation of thermal-contraction-crack polygons near Gondwana station (Germany) in northern Victoria Land (Antarctica) are reported. An area of about 20,000 m^2 characterized by random orthogonal polygons was investigated using integrated ground penetrating radar, electrical resistivity tomography, geomorphological surveys, and two trench excavations. The polygons are well developed only at elevations higher than 6–7 m above current sea level on Holocene-age raised beaches. It is concluded that the polygons are composite in nature because the shallow linear depressions that outline the polygons are underlain by fissures that can contain both sandy gravel and foliated ice (i.e., ice wedges) even in the same polygon network and at distances of just a few meters. Unexpectedly, most of the polygons follow the border of the raised beaches and develop in correspondence with stratigraphic layers dipping toward the sea, imaged by ground penetrating radar (GPR) profiles and interpreted as prograding layers toward the present-day shoreline.

KEYWORDS
electrical resistivity tomography, ground penetrating radar, ice wedges, permafrost, polygonal pattern

1 | INTRODUCTION

Polygonal patterned ground is one of the most distinctive landforms in permafrost terrain regions.[1] Polygons in arctic and subarctic areas have been intensively studied since the beginning of the last century,[2] and a wide literature exists on this topic (e.g., French[3]). Moreover, polygons associated with ice wedges and sand wedges are widespread in the ice-free areas of Antarctica.[4,5] Péwé[6] was the first who analyzed the morphology of sandwedge polygons, in the McMurdo area (southern Victoria Land). Black and Berg observed in their pioneering works[7,8] that sand wedges are more common in inland dry zones, while ice wedges are more frequent in coastal areas[9]; described thermal-contraction crack polygons in northern Victoria Land highlighting the presence of small ice wedges in the Northern Foothills. In the latter zone extensive studies of the isotopic composition and thermal regime of ice wedges have been performed.[10–12]

It is important to highlight that ice wedges are a ground ice type ubiquitous in areas of continuous permafrost, and investigating the

response of such features to climate change is helpful to understand future permafrost degradation.[13] Since ice wedges are typically encountered in the upper permafrost, polygonal terrain is particularly susceptible to thermokarst.[14] Polygonal patterned ground and ice wedges develop in a wide range of surficial materials due to thermal contraction cracking of the ground in winter and meltwater infilling of the cracks. However, the physical sensitivity of polygonal terrain varies with spatial patterns in ice-wedge size, thermal regimes, topography, and climate (e.g., Bockheim and Hall[15]). Recent warming has caused ice-wedge degradation in many sites[16] with further expected effects as a consequence of ongoing increasing warming. Therefore, since polygonal patterned ground responds in a non-linear and non-uniform manner to increasing temperatures, it is essential to fully understand all the factors involved in their origin and evolution through time. Only in this way can such features (and in particular ice wedges) be used as a proxy of climate changes.

With these objectives in mind,[1,17] found that the rate of sublimation is related to substrate and micro-topography, while Hallet et al.[1] modeled the development of sand-wedge polygons in the dry valleys of Antarctica, finding that the age was controlled by long-term rates of trough extension, and ridge growth depends on the equilibrium between sand-wedge widening and relaxation by loose sediments. On the contrary, the geometry and evolution of hexagonal or orthogonal polygonal patterns have been related to different factors, including climate, substrate, and deposit age.[18] It was further pointed out that cracks do not develop all at once, but rather new cracks are influenced by the already-existing ones, in turn resulting in a self-organizing pattern with varying angles of intersections.[19] On the contrary, Mellon et al.[20] found a strict correlation between polygon size and depth of the boundary between almost dry and ice-rich permafrost, analyzing patterns in the Antarctic dry valleys.

New approaches have been used for quantitative analysis of polygon geometry, for instance by Haltigin et al.[21] who used spatial point pattern analysis, showing that polygon networks increase in regularity with time.[22] mapped polygons using high-resolution stereo remote sensing data to extract polygon geometries on wide areas, while several methods based on different approaches, including neural network and deep learning ones, have been recently proposed for automatic or semi-automatic extraction of the polygon shape from satellite and aerial photographs.[13,23–26]

Polygonal patterned grounds raise peculiar interest also because they were found not only on the Earth surface but also on Mars, and there are several geometrical similarities between the two planets, even though on Mars they sometimes exhibit unusually wide dimensions (diameter > 100 m).[27] However, the presence of polygonal patterns on both planets suggests that thermal contraction cracking is (or was) a generic process acting in both situations. Antarctic polygons provide better terrestrial analogues of Martian polygons than Arctic polygons, due to the cold, hyper-arid environmental conditions of Antarctica; therefore, in recent years several studies focused on polygons as Mars analogues in different zones of the Antarctic continent, including Dry Valleys,[8,28] northern Victoria Land,[9,29] and Antarctic Peninsula,[30] but also in other areas of East Antarctica (e.g., Matsuoka and Hirakawa[31]).

In our study area statistical evaluations are unpractical and not meaningful due to limited extension in which the polygonal pattern develops. So, we adopted an alternative approach based on integrated morphological and geophysical investigations, the latter mainly focusing on ground penetrating radar (GPR). GPR is the most frequently used geophysical tool for imaging the internal structure of periglacial and permafrost features (e.g., previous studies[32–34]). However, up to now GPR was seldom applied to specifically image materials in areas characterized by polygonal patterns. For instance, Bode et al.[35] combined GPR and remote sensing data to estimate ice-wedge volume. Three-dimensional (3D) GPR has been successfully used for high-accuracy imaging of subsurface polygon networks[36] and ice complex deposits. Previous studies[37,38] extended 3D GPR into imaging buried networks of sediment-filled relict wedges in the USA, while Watanabe et al.[39] imaged ice and active-layer soil wedges by 3D GPR in the Svalbard, analyzing and discussing factors controlling ice-wedge distribution in a maritime, periglacial environment. 3D GPR was further used for comparative studies between Earth and Mars polygonal patterns.[40] Despite such 3D GPR examples, there are logistical constraints limiting its applicability especially when rough topography and large blocks and boulders are present at the surface.

Electrical resistivity tomography (ERT) is a geophysical technique that can be used to obtain information about variations in subsurface electrical conductivity. Since ice and frozen materials are more resistive than unfrozen and/or water saturated materials, ERT is particularly efficient in glaciological studies and specifically in permafrost systems (e.g.,[41]). As far as patterned ground and ice-wedge investigations are concerned, ERT was seldom used alone[42,43] but because of the different resolutions and sensitivities to electrical conductivity and permittivity of ERT and GPR, they can be complementary to each other and their combined use can produce novel insights.[44]

In this paper, we integrated GPR data with ERT focusing on the following objectives:

1) Analyze the relationship between polygonal patterned ground and the geological and sedimentological structures of a permafrost beach environment in northern Victoria Land.
2) Analyze polygon morphology borders where wedges are expected, by characterizing filling materials with non-destructive techniques.

2 | STUDY AREA

Within the Gerlach inlet in northern Victoria Land, very close to the Korean "Jang Bogo" and German "Gondwana" Antarctic stations, a raised beach studied since the first Italian Antarctic expeditions[45,46] rests directly on bedrock (mainly gneiss of the Wilson Terrane,[47] Figure 1). According to,[48] at least 12 prominent beach ridges can be recognized up to 30 m asl, and the rates of emergence range from <2 mm yr^{-1} in the last 3 kyrs to >10 mm yr^{-1} for the oldest beaches (ca 7,500 yrs BP). The analyzed beach is within a continuous permafrost area, although characterized by a quite thin high resistivity permafrost layer overlying low resistivity values.[49] Geomorphologically,
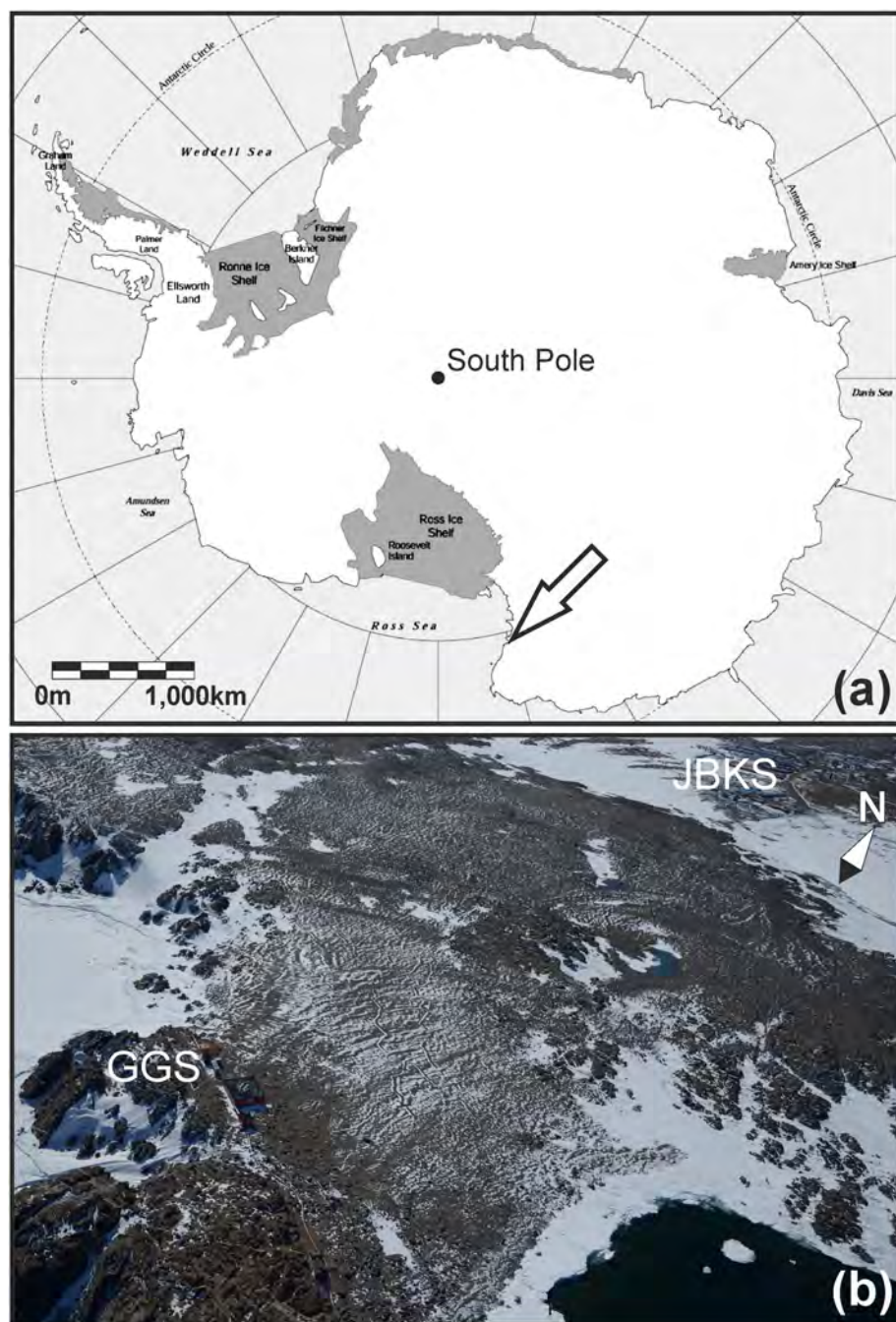
FIGURE 1 (a) Location map; (b) aerial photograph of the study area. JBKS and GGS labels refer to the Jang Bogo (Korean) and Gondwana (German) stations, respectively [Colour figure can be viewed at wileyonlinelibrary.com]

the beach is also characterized by the occurrence of abundant "ventifacts" that testify the strong catabatic winds flowing in this area for a large part of the year.[50] Climate is arid and very cold with a mean annual air temperature (MAAT) of −14.0°C at Baia Terra Nova,[51] and an annual net precipitation (precipitation minus evaporation) of less than 100 mm yr−1.[52]

3 | METHODS

Geophysical data were collected on November 3, 2014. GPR is a geophysical technique exploiting the propagation of electromagnetic

(EM) waves produced by antennas to image underground electromagnetic property contrasts and reconstruct their geometries. The GPR acquisition was made by using a ProEx GPR instrument (Malå Geoscience) connected with 250 MHz shielded antennas, selected after preliminary tests done with higher central frequencies (500 and 800 MHz) antennas that gave worse results due to limited penetration depth and higher overall scattering related to the size of stones on and below the surface (see Figure 2). In addition, in the case of lower frequency antennas (which are always bigger in size) the rough surface produces a worse coupling with more diffractions responsible for an overall lower signal-to-noise ratio. The GPR instrument was triggered by an electro-mechanical odometer allowing a constant trace

FIGURE 2 Photograph of the study area in November 2014 taken during the geophysical data acquisition. Borders of polygonal patterns are emphasized by snow accumulation and are pointed by the yellow arrows. In the foreground is seen a portion of the ERT equipment. View from south to north [Colour figure can be viewed at wileyonlinelibrary.com]
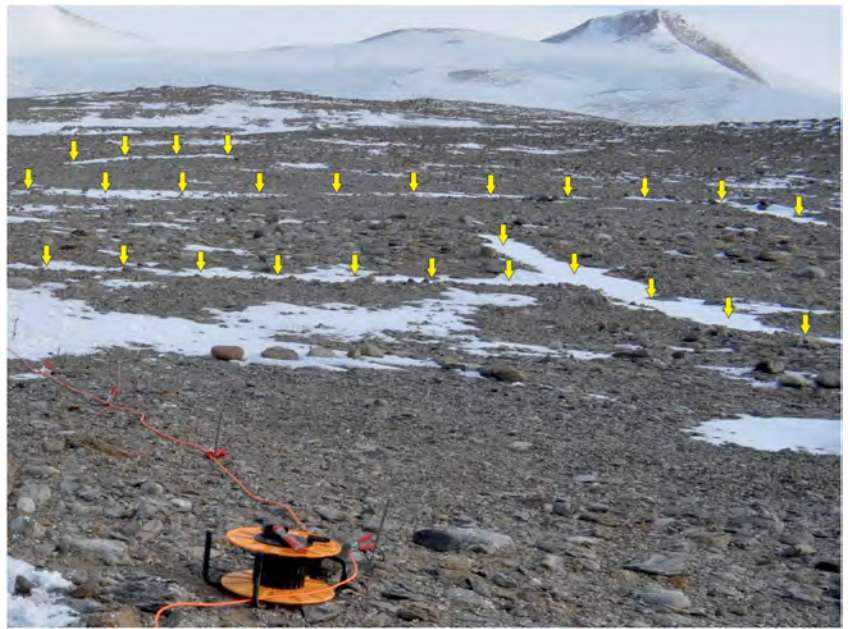
interval equal to 0.05 m, while absolute positioning was assured by a portable differential global positioning system (DGPS) Magellan ProMark 3 with decimetric absolute accuracy. Ten sub-parallel NW-SE GPR profiles were collected, reaching a total length of 2040 m (Figure 3). The applied GPR processing flow included DC removal, zero-time correction (drift removal), spectral analysis and bandpass filtering, geometrical spreading correction, exponential amplitude correction, diffraction velocity analysis, depth conversion, and 2-D migration (Stolt algorithm). Due to the limited number of clear and non-interfering diffractions, a constant velocity field was used for depth conversion with a velocity equal to $0.16\,\mathrm{m\,ns^{-1}}$. We preferred to interpret unmigrated profiles because diffractions were used as an aid to locate interruptions of the reflectors and other distinctive features related to the polygons. To better understand the signature of GPR signal we exploited some GPR attributes and in particular the trace envelope (instantaneous amplitude), the cosine of the instantaneous phase, the dominant frequency, and the sweetness. Sweetness is a composite attribute calculated as the ratio between the instantaneous amplitude and the square root of the instantaneous frequency. A detailed analysis of the meaning of such attributes is out of the scope of this paper, but a comprehensive analysis related to glaciological application can be found in.[53]

ERT encompasses two partially superimposed profiles, collected with a Pasi system in Wenner configuration. Each profile has 64 electrodes, 2 m spaced and a superimposition equal to 16 electrodes (Figure 2). Therefore, the total concatenated profile length equals to 220 m. From a total of 1,302 apparent resistivity measures 1,067 have been selected for data inversion. We decided to exclude several measures on the basis of different criteria, namely, the effective electric current, the voltage, the standard deviation between reciprocal measures, and the presence of outliers considering the values of a single measure in comparison with the surrounding ones. Data inversion was achieved with RES2DINV (Geotomo software) selecting a combined

Marquardt and Occam inversion approach and a robust constrain (L1-norm) on the model resistivity,[54] to decrease the effect of noisy data, which are expected in a high resistivity context as in the present case. With these settings we obtained global root mean square (RMS) errors below 5%, which is quite satisfying considering the very high resistive shallow materials which often increase the resistance of contact.

Geomorphological analyses were accomplished by inspecting the area, analyzing existing aerial/satellite photographs, and mapping the position and elevation of the two terraces (T1 and T2) as well as the upper limit of the beach (Tab) using the same GPS unit used for GPR and ERT acquisitions. In addition, two previously excavated trenches (located by red and yellow squares in Figure 3) were used to describe the morphology of the wedges and their infilling material, with the aid of a jackhammer.

4 | RESULTS

Polygons at the surface are visible (and made more apparent by the differential snow accumulation) in an area of approximately 240 m by 80 m (i.e., about 2 hectares) elongated in SSE–NNW direction (Figure 3). The pattern of the polygon is random orthogonal with a maximum diameter of ca. 25 m.

Among the 12 beach ridges identified by Baroni and Orombelli[48] two of them are particularly evident (T1 and T2 in Figure 3) in the zones where the polygons have been detected. Of the 37 intersected polygons borders, 11 were intercepted by the GPR profiles at elevations lower than T1 (7–8 m asl); they are all related to the polygons showing the smaller diameter. Twelve polygons are located at elevations between T1 and T2, while just one wedge was intercepted by GPR profiles at elevations higher than T2 (11 m asl). In addition, it is interesting to notice that four points are just along the T1 limit, while
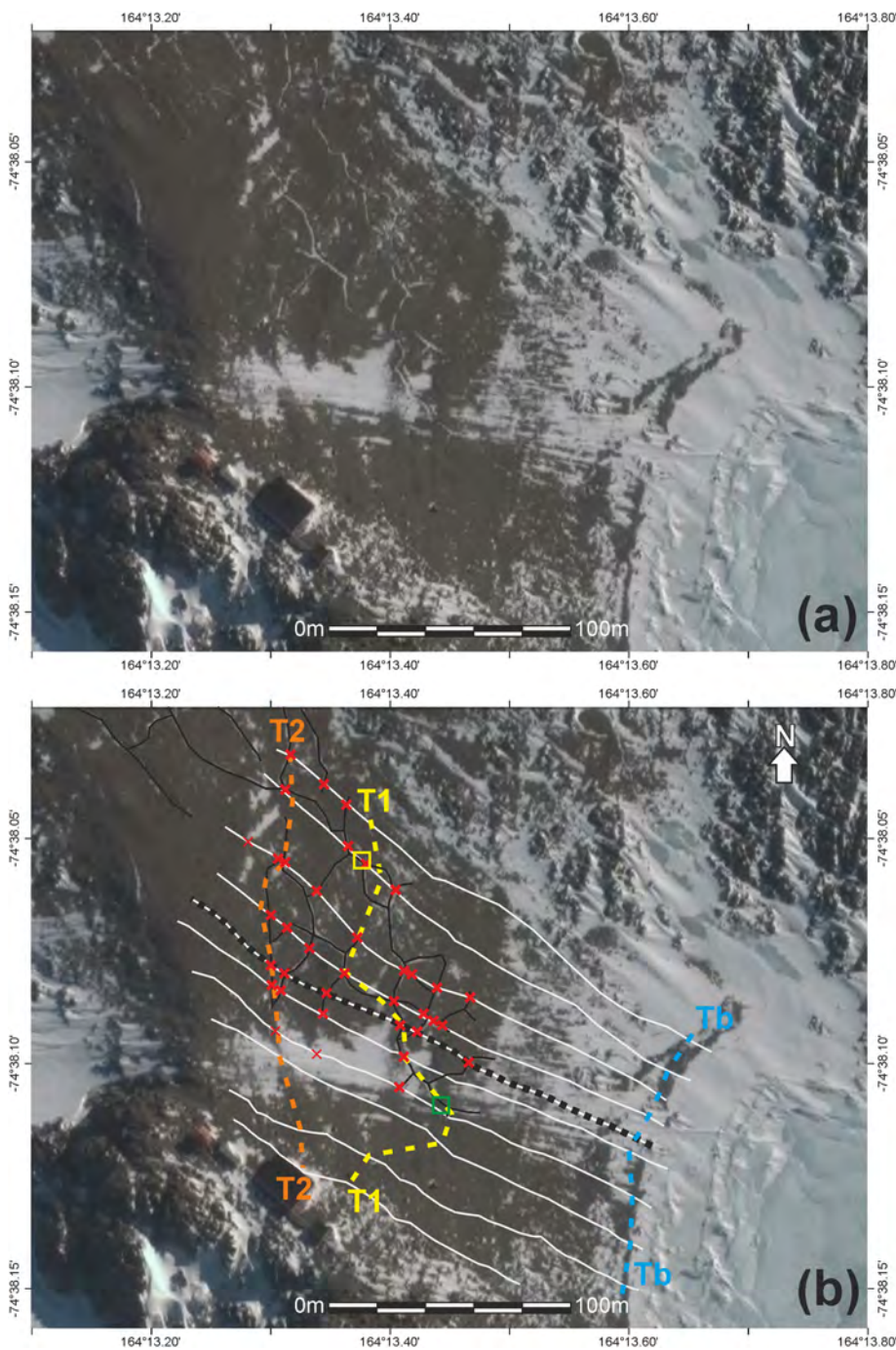
FIGURE 3 (a) Georeferenced satellite image collected in November 2014 with (b) geophysical data survey location and main geomorphological structures superimposed. White lines and black dots mark ground penetrating radar (GPR) and electrical resistivity tomography (ERT) profiles, respectively. Black lines are the GPS paths of the polygons recognized on the field, while thick-red crosses mark intersections with GPR profiles and thin-red crosses show polygons not recognized on the field due to the snow cover. T1 and T2: Main beach ridges; Tb: Top of the current berm. The location of an ice-wedge excavation is indicated by the yellow square, while the frost fissure excavation is marked with the green square.[9] Map data: Google, Maxar Technologies, November 2014 [Colour figure can be viewed at wileyonlinelibrary.com]

six others are along (or very close to) the T2 limit. In Figure 3 it is also apparent that several borders of the polygons follow the limits of both T1 and T2. For completeness in Figure 3 we also map the top of the current berm (Tb), which has an elevation of 1–1.5 m asl.

In our study area, the ramps along the borders are usually just a few centimeters up to a maximum width of 20 cm with a height of a few centimeters, while the furrow is also from a few centimeters to 15–20 cm deep (Figure 2). More accurate and precise measures were not possible due to the very rough surface with several blocks and variable size stones (Figure S1 supplementary) and due to the snow often present inside the furrows.

Initially, we compared results obtained by ERT and GPR along the same path (Figure 4). The electrical resistivity has a very wide range (from 5×10^1 up to 1×10^5 Ωm) and an interesting general trend, with the highest values at and near to the surface and a downward decreasing trend, as observed by.[49] Close to the current berm (SE side of the profile) the resistivity shows an opposite tendency: at the surface there are materials characterized by hundreds of Ωm, while just a few meters below the resistivity increases to tens and thousands of Ωm suggesting frozen materials (and even massive ice) and permafrost conditions. The thickness of the high resistivity zone increases up to 10–15 m toward NW. Where the ERT profile crosses the polygon

FIGURE 4 Ground penetrating radar (GPR; top) and electrical resistivity tomography (ERT; bottom) profiles collected along the same path (see Figure 3 for location). ERT inversion has RMS % error equal to 4.9 after five iterations. Tab label marks the top of the current berm. Red crosses show the location of the borders of polygons intercepted by the profile. Black dashed and light blue dotted lines correlate terraces and polygons on GPR and ERT profiles, respectively. Light blue dashed lines mark some of the dipping horizons imaged by GPR. Scales of GPR and ERT are identical; vertical exaggeration 2x [Colour figure can be viewed at wileyonlinelibrary.com]
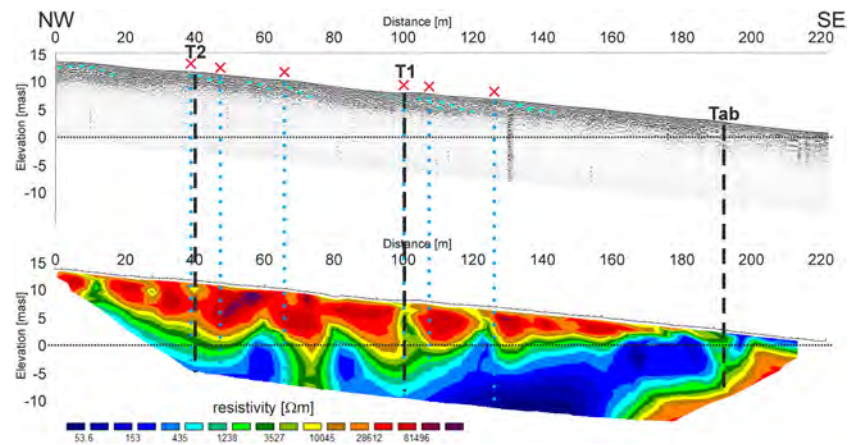
borders (light blue dotted lines in Figure 4) there is a resistivity lowering in the shallowest portion, sometimes moderate (i.e., about half of the surroundings), and sometimes very high (up to two orders of magnitude). We have to remark that the electrode spacing was equal to 2 m, giving accurate results starting from about 1 m below the topographic surface. Another noticeable behavior is that the resistivity decreases at the beach ridges (T1 and T2) and that in these zones there are more polygon borders (Figures 3 and 4). Close to the actual sea side (i.e., toward SE) in the shallower part there are resistivities below 100 Ωm probably due to salt water–saturated sediments. In the same zone, just below the mean sea level elevation the resistivity increases up to thousands Ωm, values that could be attributed to permafrost conditions below the sea bottom, but further data must be considered to verify such an hypothesis, which is far from the subject of this paper. In any case, such resistivity trend is real and not related to inversion border effects as demonstrated by the comparison between apparent and real resistivity models (Figure S3 supplementary).

Since the GPR maximum penetration depth does not exceed 4–5 m, we focused on the shallower portion to better understand polygons' development and interaction with the other morphological and geological elements. One of the most evident features imaged by GPR is a series of reflectors dipping toward the sea side with an apparent dip up to 25°–30° since the data are not migrated.

Figures 5 and 6 show a portion of interpreted GPR profiles crossing the lower (T1) and the upper (T2) main beach ridges, respectively.

Attributes are helpful in the interpretation process since they emphasize some data characteristics. For instance, the cosine of the instantaneous phase allows us to follow reflectors by exploiting their lateral phase behavior even when the reflection amplitude (as well as all the amplitude-related attributes) is discontinuous. On the contrary, the sweetness allows us to highlight zones having a similar GPR signature, since it is an attribute that combines together amplitude and spectral characteristics of the signal.

In the study area, we interpreted three main GPR reflectors having different characteristics, geometries, and EM signature highlighted by attribute analysis. In particular, a high-reflective and continuous horizon (H1), sub-parallel to the topographic surface (yellow dashed line in Figures 5 and 6), lies at depths between 30 and 80 cm. Seaward (i.e., SE) dipping horizons (H2) reaching a maximum apparent dip equal to 30° never intersecting each other and with moderate to very high reflectivity and variable lateral continuity (light blue dashed line in Figures 5 and 6) are present in the higher portion of the study area. In addition, a discontinuous sub-horizontal or gently dipping horizon (H3) lying 2.5–4.5 m below the surface (orange dashed line in Figure 5) was recognized.

After this global interpretation of the structures imaged by GPR, we focused on the EM signature in correspondence with the polygon borders mapped at the surface. Figure 7 provides an example of two neighboring polygon limits, as well as further details of the previously described horizons. The shallowest horizon (H1, yellow dashed lines) is interpreted as the frost table and interrupts in correspondence to the polygon borders (red crosses). Polygon borders lie in correspondence to emerging dipping layers, which stop on a sub-planar horizon showing high lateral continuity (H3, orange dashed lines) as clearly shown especially by the cosine of the instantaneous phase attribute. Just above some borders there are lenses of fine sediment, usually 1 to 3 m wide (white dashed line) most likely representing aeolian deposits. In between dipping horizons and in correspondence to the borders, there are zones with peculiar GPR signatures (yellow transparent zones in Figure 7), highlighted by the integrated attribute analysis. From the exemplary data in Figure 7, we can notice zones with low and chaotic reflectivity, no lateral continuity, and abrupt lateral terminations, in between regularly layered facies.

5 | DISCUSSION

5.1 | Relationship between the polygonal patterned ground and the geological/sedimentological structures

GPR horizons can be interpreted on the basis of their EM signature, geometry, correlation with surface morphology, and literature data.

Horizon H1 can be interpreted as the frost table, as suggested in[55] for an area close to the sea and less than 20 km to the south from
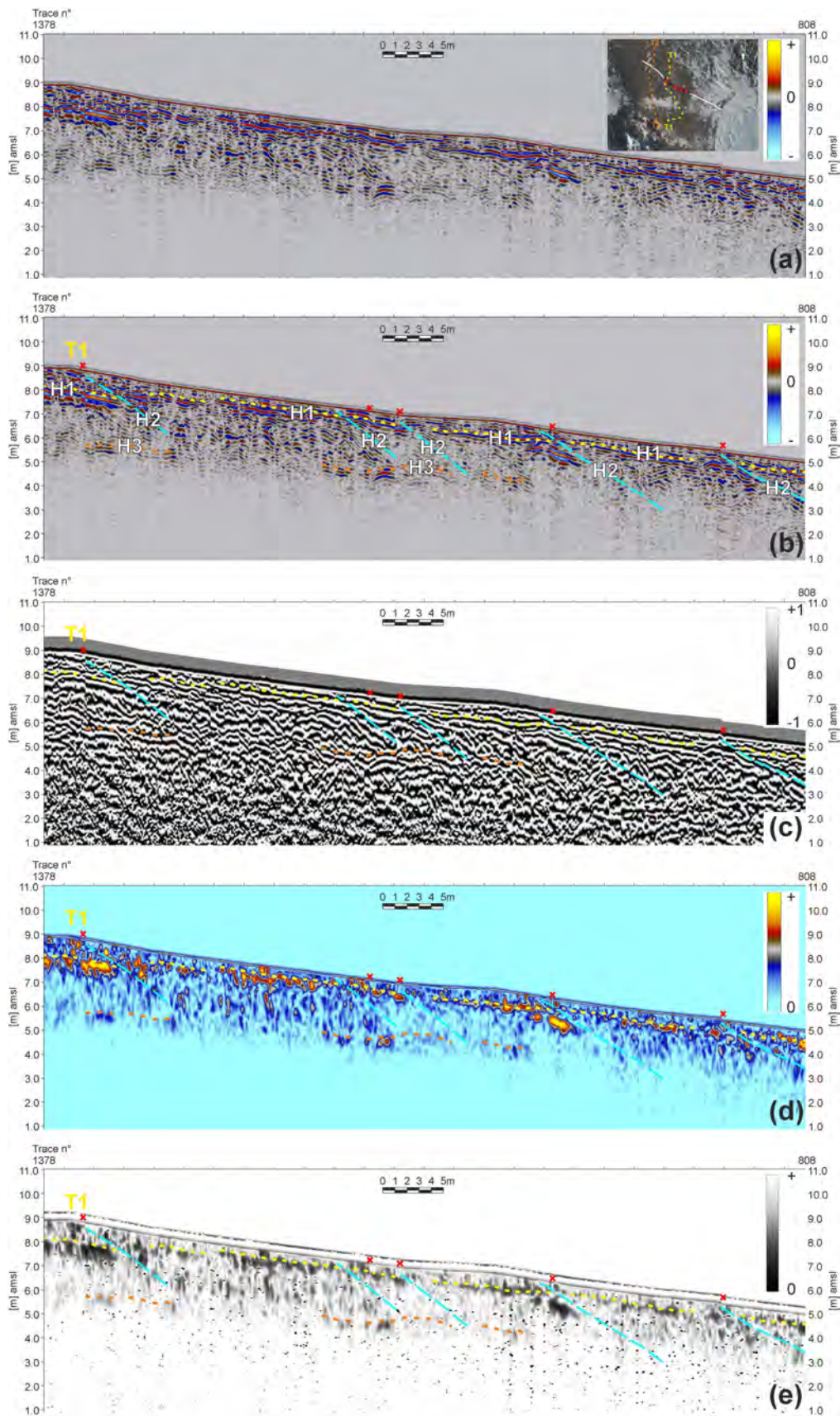
FIGURE 5 Portion of (a) uninterpreted and(b, c, d, e) interpreted ground penetrating radar (GPR) profile crossing the lower main beach ridge (T1). Location in (a). Reflection amplitude (a, b); cosine of instantaneous phase (c); trace envelope (d); sweetness (e). Red crosses show the location of polygon borders. Vertical exaggeration 2x. See text for the description of horizons [Colour figure can be viewed at wileyonlinelibrary.com]

Gondwana station. It is, as expected, almost parallel to the topographic surface and in some places is laterally continuous, while in others it exhibits an irregular signature. This horizon is interrupted at the polygon sides (Figures 5, 6, 7, 8) where there is always a strong phase discontinuity emphasized by the cosine of phase attribute. This confirms the pattern of soil temperature found by[56] just some hundred meters away from the study area, which measured ground surface temperatures at the borders of some (albeit smaller) polygons up to 2.8°C warmer than at the centers. However, it can be also explained by a coarser material enhancing the scattering and/or to limitations in GPR imaging of the steeply dipping frost table reflector deepening at polygon borders. In any case, the geophysically estimated frost table depth is in agreement with,[57] which reported an active layer thickness ranging from 2 to 92 cm in unconsolidated deposits (while it exceeds 1.6 m in granitic bedrock).

Horizons H2 are seaward-dipping reflectors mapped along all the central profiles, while they are not present in the two southernmost profiles (Fig. suppl. S2) where the bedrock is almost outcropping (Figures 1, 3). As a consequence of that, they can be interpreted as prograding sedimentary levels related to different beaches, raised during the Holocene.[9,48] They locally deviate from the general SE dipping trend, with deformations and more complex geometries (Figure 7).

Horizon H3 is not continuous in the study area and locally disappears in the central and northern profiles, while it is not present in the southernmost ones (Fig. suppl. S2). It is most probably interpreted as the top of the bedrock below the sedimentary levels, although we cannot exclude that it could be related to different (probably glacial) older sediments.

Besides all the usually considered factors driving and influencing the polygon development such as climate, substrate grain size, deposit age, active layer geometry, permafrost characteristics, and hydrology, we found that most of the polygons borders in our study area develop at beach ridges (i.e., borders of terraces), (Figure 3) and/or where some preexisting stratigraphic layers reach the topographic surface (Figures 4–7). This is a remarkable result because in a limited area, as the one selected for the study, most of the other factors are constant or very similar.

The analyzed polygons have narrow borders and null to decimetric furrows and therefore are difficult to be studied by any geophysical method. We, therefore, focused on GPR technique, which provides a resolution that is higher than that of the other available geophysical techniques.[58] GPR surveys to study ice wedges are quite common in the literature (e.g.,[59,60]), but all these cases seem to be considerably different both in terms of wedge scale and physical characteristics from our case study. In fact, most of the studies focus on the Arctic where ice wedges typically are several meters wide, with depths exceeding 10 m and well developed on areas of tens or even hundreds square kilometers (e.g.,[13]). Quite surprisingly, in[61] we found wedges with an EM signature similar to the ones analyzed here (see Figure 20 therein). The main objective of that study was to determine the near-subsurface structure and the distribution of buried ground ice in the permafrost within Haughton impact Crater in northern

Canada (75°23' N; 89°40' W), used to simulate a lunar mission. As in our study, the EM signature of the polygon borders is spatially variable, but distinctive, with the local interruption of the frost table, which lies at depths between about 1 and 2 m. However, the geological and geomorphological setting is very different from our study area since within the crater there are mainly carbonates and carbonate breccias covered by thermally derived, poorly sorted angular rocks ranging from a few centimeters to 5 mm in size.[61]

Although beyond the specific aims of this paper, we can make some preliminary estimates of the chronology of the polygons, which are present only at elevations above 6–7 m higher than the present sea level. Assuming the maximum uplift rates proposed by Baroni and Orombelli,[48] which are equal to 2 mm yr^{-1} for the last 3,000 years and 10 mm yr^{-1} before, the minimum age for the polygon formation is ca. 3,300 years BP. We should also consider that at around 15 m asl (i.e., about 4,000 years BP with the same uplift rates) on this beach French and Guglielmin,[50] analyzing the honeycomb weathering and the wind abrasion on the widespread ventifacts, estimated an erosion rate of about 0.001 mm yr^{-1} i.e., roughly an order of magnitude lower than 0.015–0.022 mm yr^{-1} recorded by Spate et al[62] for the Larsemann and Vestfold Hills, in Eastern Antarctica, or than 0.002–0.012 mm yr^{-1}[63,64] reported in Western Antarctica. This lower erosion can be explained by an older age of the sediments that was documented more southward at Cape Ross by Gardner et al[65] where beaches consist primarily (or even entirely) of material that predates the Holocene.

5.2 | Characterization of the infilling wedges material

Generally, wedges in Antarctica are small: about 1 m wide in the dry valleys[6] and 0.5–1.5 m deep and 0.1–0.5 wide in northern Victoria Land.[9] In continental Antarctica sand wedges and frost fissures (or tessellations according to[9]) are relatively widespread in areas not perennially covered by ice, being most common in the dry valleys and the later in northern Victoria Land. The presence of ice wedges in vast areas of northern Victoria Land was reported by[66] but here we focus on an ice wedge found by one of the authors (R.R.) and a frost fissure already discussed in[9] filled by an openwork matrix of stones and pebbles, suggesting lateral slippage into the crack (both located in Figure 3).

We remark that while some borders exhibit transparent zones just below their emergence at the surface, others are, in contrast, characterized by strong reflections and diffractions (Figure 8). Most of the borders are in correspondence with stratigraphic layers dipping toward the sea and with the beach ridges T1 and T2 (Figures 5–8). Since we acquired GPR profiles almost perpendicular to the seashore, they should therefore intersect the stratigraphic structures nearly perpendicularly, but even when known from surface observation, lateral correlations show different geophysical characteristics in terms of reflection amplitudes, EM transparency, and lateral phase continuity, as apparent in Figure 8. From the geophysical data it is impossible to
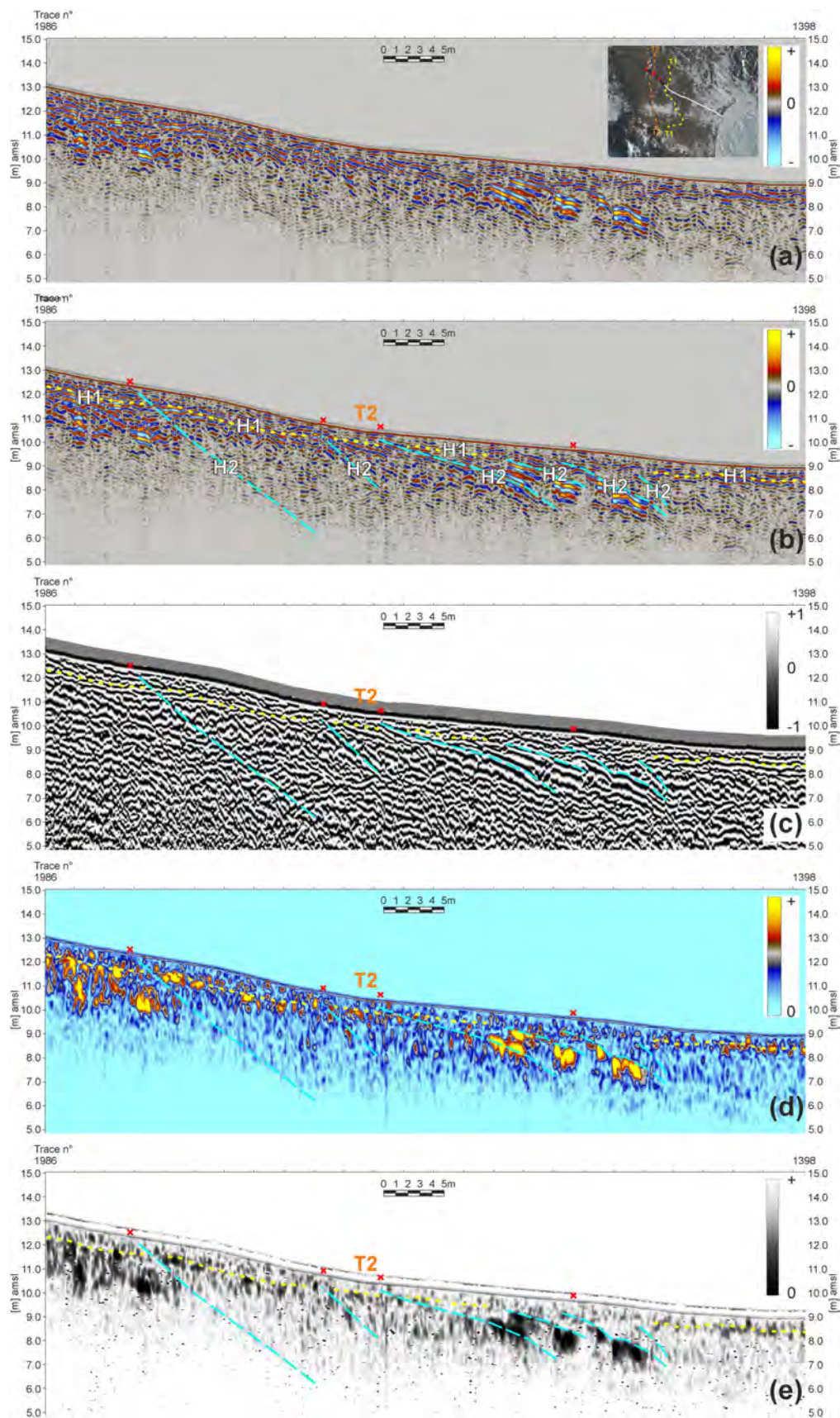
FIGURE 6 Portion of (a) uninterpreted and (b, c, d, e) interpreted ground penetrating radar (GPR) profile crossing the higher main beach ridge (T2). Location in (a). Reflection amplitude (a, b); cosine of instantaneous phase (c); trace envelope (d); sweetness (e). Red crosses show the location of polygon borders. Vertical exaggeration 2x. See text for the description of horizons [Colour figure can be viewed at wileyonlinelibrary.com]

FIGURE 7 Details of (a) uninterpreted and (b, c, d, e) interpreted ground penetrating radar (GPR) profile crossing lower terrace (T1). Location in (a). Reflection amplitude (a, b); cosine of instantaneous phase (c); sweetness (d). Red crosses show the location of two polygon borders. No vertical exaggeration. Yellow, light blue and orange lines mark the same horizons as in figures 5 and 6, while shallow white dashed line and yellow transparent areas are discussed in the text [Colour figure can be viewed at wileyonlinelibrary.com]
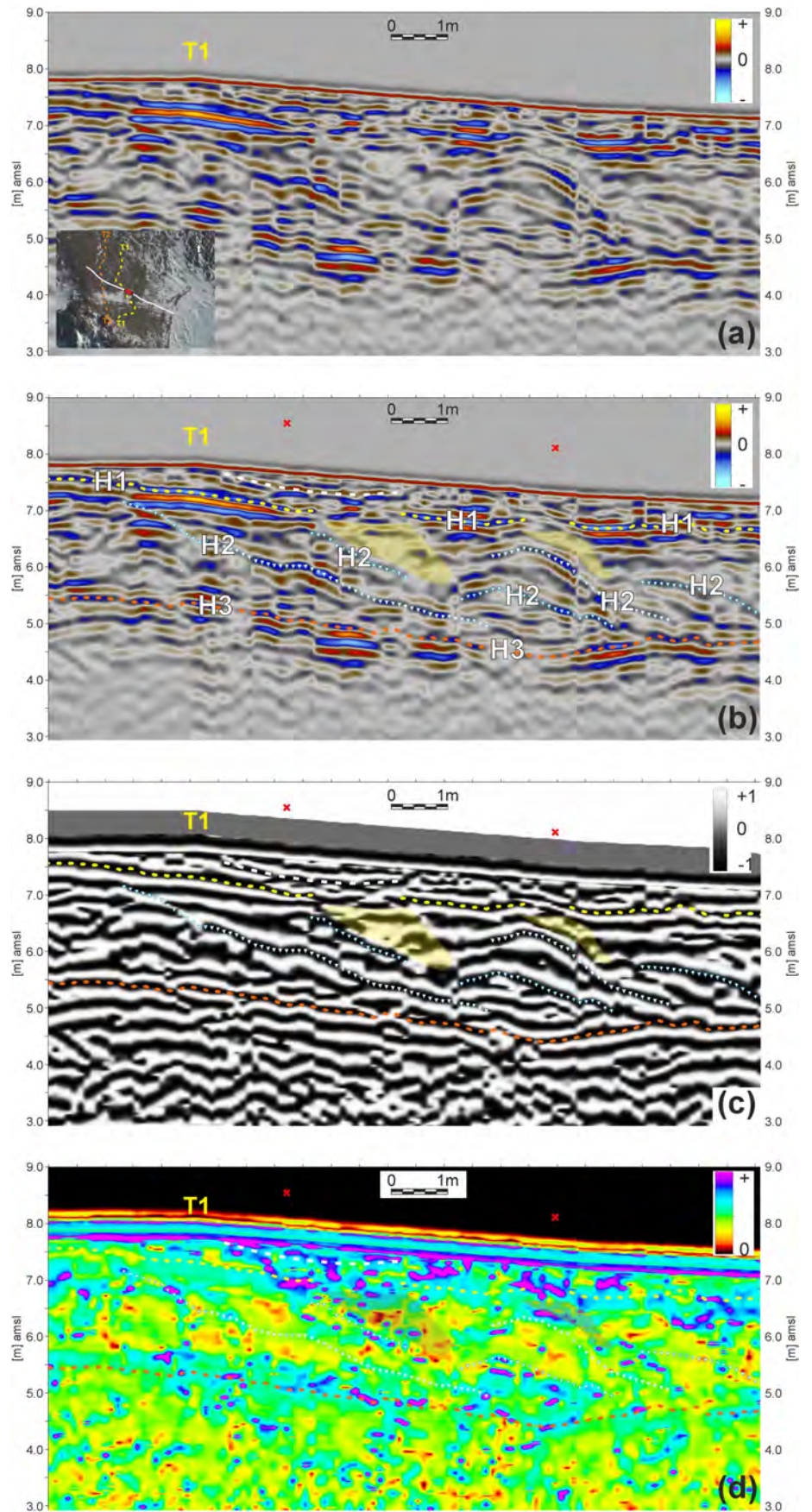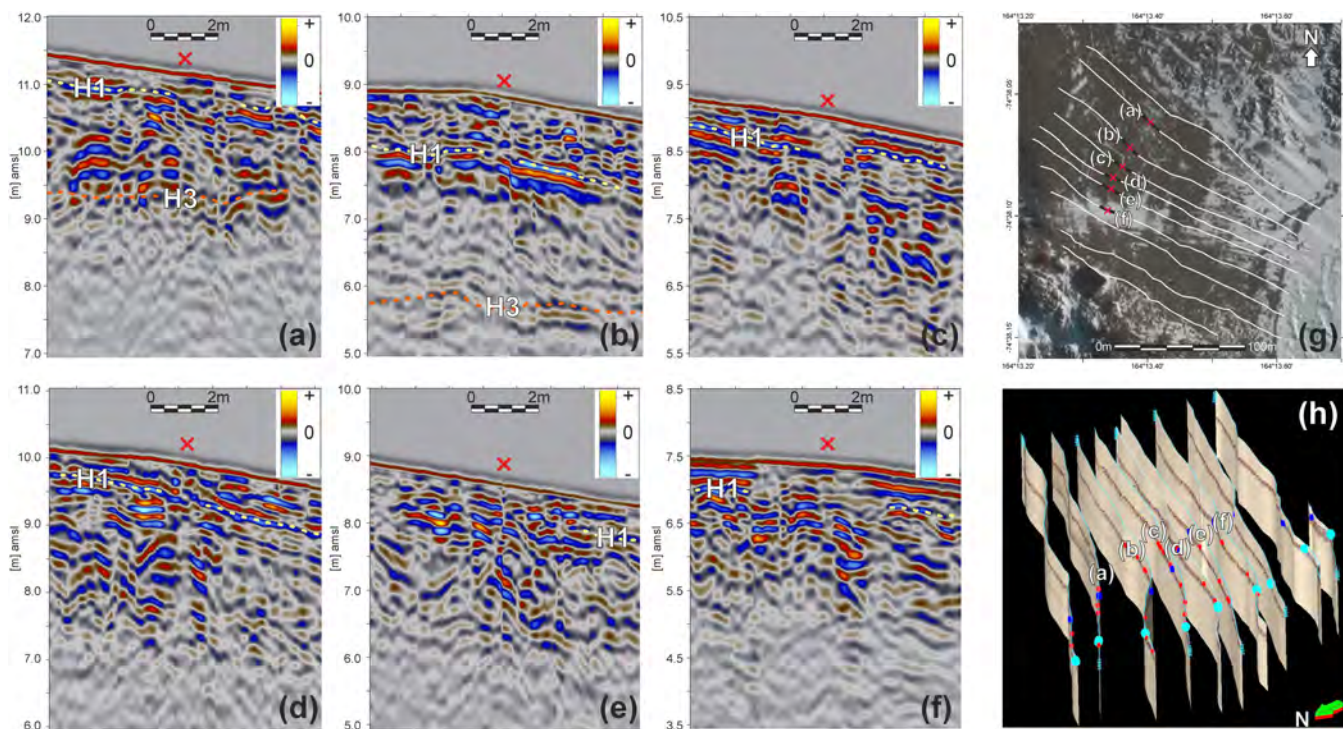
FIGURE 8 Lateral correlation of the polygons on selected portions of adjacent profiles (a–f, from north to south). Only H1 and H3 horizons are here shown. (g) Location map of pictures from (a) to (f); (h) 3-D perspective view of all the GPR profiles with the positions of polygons' borders (red dots), T1 beach ridge (blue dots), and T2 beach ridge (light blue dots) superimposed [Colour figure can be viewed at wileyonlinelibrary.com]

recover the actual shape of the wedges. Indeed, they are probably irregular and not homogeneous even for small lateral distances; however, their extension in depth can be estimated in 1–1.5 m below the topographic surface. From our results it is apparent that polygons develop only when the sediments have enough thickness, and in fact no polygons are present to the south (and to north-east) of the study area, where the bedrock is almost outcropping (Fig. suppl. S2).

In Figure 9 we compared the logs of the two wedges excavated in December 2000 and 1998 (red and yellow squares in Figure 3, respectively) with the closer GPR profiles, crossing the border of two polygons just a few meters apart. We can infer that even if the vertical and lateral resolution of GPR data is not sufficient to image wedge details as in the excavations, the EM signature suggests the presence of a peculiar structure in correspondence of both the trenches, i.e., the ice wedge (Figure 9a) and the frost fissure (Figure 9c). In particular, the frost table, which is usually very continuous on GPR data (yellow dotted lines in Figure 9a and 9c), is interrupted in correspondence to both the ice wedge and frost fissure and occurs roughly at the same depth of the observed trenches and in the range found almost everywhere in northern Victoria land by Raffi and Stenni.[10] The ice does not have a distinctive signature on GPR data due to the limited lateral extension of the wedges and the resolution of GPR signal. The geometry of ice wedges and especially their lateral sub-vertical limits cannot be accurately imaged on GPR data as reported also by,[67] but its presence and location can be indeed detected on GPR data. The lateral limits of the frost fissure are clearer with a distinct phase interruption, possibly because of their lower dip. Below the frost fissure the signal amplitude is generally lower than in the other zones of the profiles at the same depth; this in turn can be due to higher EM attenuation of the materials filling the frost fissure.

In general, the following tentative interpreting criteria to discriminate ice wedges and frost fissures can be proposed:

1. Ice wedges should produce abrupt lateral phase changes due to the high reflectivity contrast and, possibly, low attenuated signals due to the low attenuation typical of clean ice, but different types of ice can produce very different signals[67,68];
2. Frost fissures (i.e., wedges with the parent sediments inside) could have higher attenuation and possible internal layering due to different deformations that led to a secondary iso-orientation of the clasts and the sandy materials.

With this in mind and by exploiting the geophysical data validation at the two trenches locations, we infer that in the entire study area, while the polygon borders are quite clear, continuous, and well developed, the filling materials can be different even at lateral distances of just a few meters and in the same polygon network, with portions in which ice wedges are present, and other characterized by mainly sandy sediments with some pebbles filling the fissures.
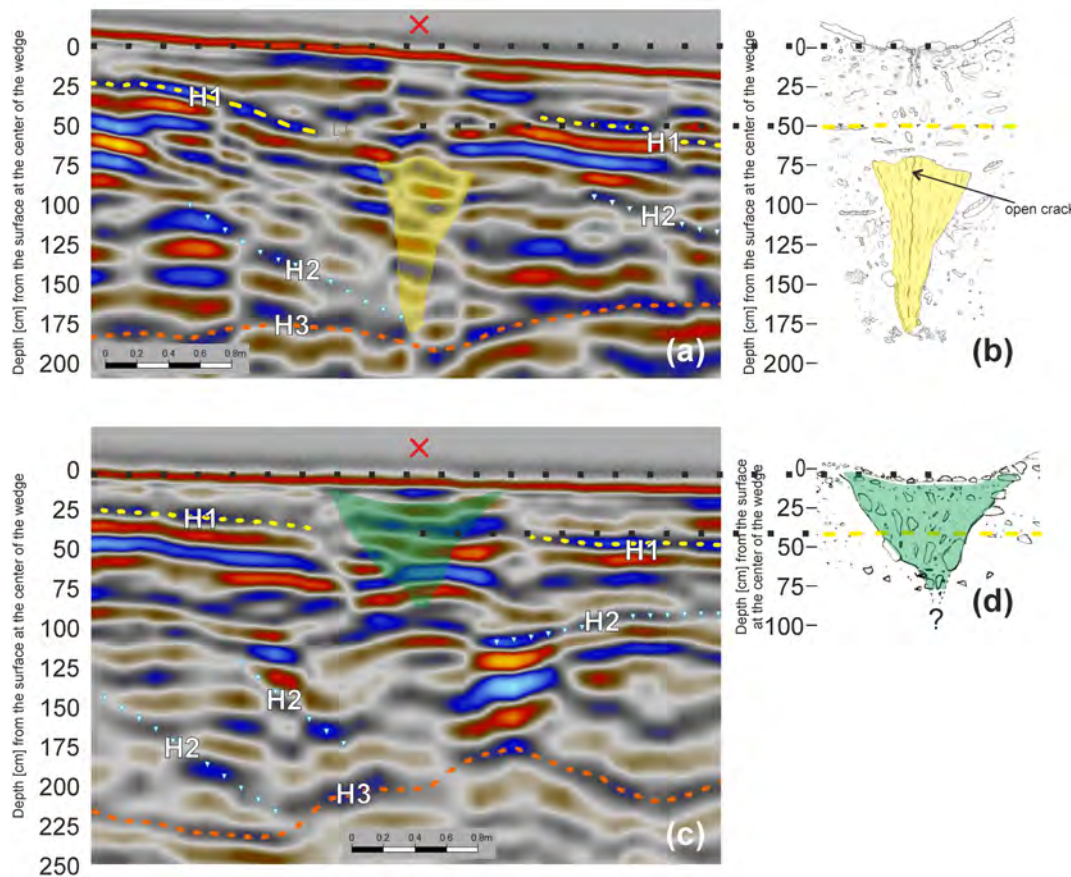
FIGURE 9 Comparison between a portion of the ground penetrating radar (GPR) profiles closer to the ice wedge dug in (a) December 2000 and (c) in 1998 and (b) the logs of the excavation (original draw) and (d) (French and Guglielmin,[9] modified), respectively. Yellow dashed lines mark the frost table, while all the other GPR horizons have the same meaning as in Figures 6 and 7. The yellow zone representing the ice wedge foliation in (b) is superimposed on (a) for comparison, while the green zone marking the limits of the frost fissure in (d) is superimposed on (c) for comparison. Vertical and horizontal scales are identical as well as scales of all the pictures [Colour figure can be viewed at wileyonlinelibrary.com]

6 | CONCLUSION

From this integrated data analysis, we can conclude that integrated electrical and GPR geophysical techniques can be used to derive spatial information on polygonal patterned ground correlating geomorphological data and trench logs. Specifically, within the study area, polygons can develop only where there is a minimum sediment thickness of roughly 1–1.5 m and are present only at elevation above 6–7 m higher than the present sea level: assuming the maximum uplift rate proposed by,[48] a minimum age of 3,300 years BP is obtained, although we cannot exclude that the sediments predate the Holocene.

From the GPR point of view, the borders of polygons can be always imaged by abrupt lateral phase and amplitude variations and by the local interruption of the frost table horizon, which is, on the contrary, quite continuous elsewhere. This is in agreement with ground surface temperatures collected within polygons borders just few meters from the study area. From the electrical point of view, polygon borders always show a decrease in resistivity with various magnitudes as compared to the surrounding materials. This is most probably due

to the filling sediments that could be finer than that characterizing the uplifted beaches.

The filling materials can be different even at lateral distances of just a few meters and in the same polygon network, but the relatively small dimension of such structures and the limited resolution of GPR prevent a precise material characterization.

We demonstrated that polygon borders are strongly influenced by both preexisting internal layering of the sedimentary materials and by morphological structures like uplift beach ridges. As a consequence, further studies focused on polygon development and evolution should consider preexisting stratigraphic layers and structures as additional driving elements in addition to many other factors like climate, substrate grain size, deposit age, permafrost characteristics, and hydrology.

DATA AVAILABILITY STATEMENT

The data that support the findings of this study are available from the corresponding author upon reasonable request.

ORCID

Emanuele Forte   https://orcid.org/0000-0002-5995-9254
Hugh M. French   https://orcid.org/0000-0001-5704-0351
Ilaria Santin   https://orcid.org/0000-0003-3566-2189
Mauro Guglielmin   https://orcid.org/0000-0002-5966-9572

REFERENCES

1. Hallet B, Sletten R, Whilden K. Micro-relief development in polygonal patterned ground in the Dry Valleys of Antarctica. *Quatern Res*. 2011; 75(2):347-355. doi:10.1016/j.yqres.2010.12.009
2. Leffingwell EDK. Ground-ice wedges, the dominant form of ground-ice on the north coast of Alaska. *J Geol*. 1915;2(3):3-635. doi:10.1086/622281
3. French HM. *The periglacial environment*. Fourthed. Hoboken, NJ, USA: John Wiley and Sons; 2017 515pp. ISBN 978-1-119-13278-3. doi:10.1002/9781119132820.
4. Bockheim JG. Permafrost distribution in the Southern Circumpolar Region and its relation to the environment: a review and recommendations for further research. *Permafr Periglac Process*. 1995;6(1):27-45. doi:10.1002/ppp.3430060105
5. Bockheim JG, Hall KJ. Permafrost, active-layer dynamics and periglacial environments of continental Antarctica. *S Afr J Sci*. 2002;98:82-90.
6. Péwé TL. Sand wedge polygons (Tessellations) in the McMurdo Sound Region, Antarctica-A progress report. *Am J Sci*. 1959;257(8):545-552. doi:10.2475/ajs.257.8.545
7. Berg TE, Black RF. Preliminary measurements of growth of non sorted polygons, Victoria Land, Antarctica. In: Tedrow JCF, ed. *Antarctic Soils and Soil Forming Processes*. Antarctic Research Series. Vol.8. Washington, DC: American Geophysical Union; 1966:61-108. doi:10.1029/AR008p0061.
8. Black RF, Berg TE. Hydrothermal regimen of patterned ground, Victoria Land, Antarctica. Proceedings: *International Association of Scientific Hydrology*. General Assembly of Berkeley 1963 - Snow and Ice. Publication 61. 1963:121-127.
9. French HM, Guglielmin M. Frozen ground phenomena in the vicinity of Terra Nova Bay, Northern Victoria Land, Antarctica: a preliminary report. *Geogr Ann*. 2000;82(4):513-526. doi:10.1111/j.0435-3676.2000.00138.x
10. Raffi R, Stenni B. Isotopic Composition and Thermal Regime of Ice wedges in Northern Victoria Land, East Antarctica. *Permafr Periglac Process*. 2011;22(1):65-83. doi:10.1002/ppp.701

11. Raffi R, Stenni B, Flora O, Polesello S, Camusso M. Ice wedge evidence in the Mesa Range (Northern Victoria Land, Anctartica). *Terra Antartica Rep*. 2003;8:149-152.
12. Raffi R, Stenni B, Flora O, Polesello S, Camusso M. Growth processes of an inland Antarctic ice wedge, Mesa Range, northern Victoria Land. *Ann Glaciol*. 2004;39:379-385. doi:10.3189/172756404781814195
13. Bernard-Grand'Maison C, Pollard W. An estimate of ice wedge volume for a High Arctic polar desert environment, Fosheim Peninsula, Ellesmere Island. *Cryosphere*. 2018;12(11):3589-3604. doi:10.5194/tc-12-3589-2018
14. Jorgenson MT, Shur YL, Pullman ER. Abrupt increase in permafrost degradation in Arctic Alaska. *Geophys Res Lett*. 2006;33(2):L02503. doi:10.1029/2005GL024960
15. Kokelj SV, Lantz TC, Wolfe SA, et al. Distribution and activity of ice wedges across the forest tundra transition, western Arctic Canada. *J Geophys Res*. 2014;119(9):2032-2047. doi:10.1002/2014jgrf.003085
16. Wolter J, Lantuit H, Wetterich S, Rethemeyer J, Fritz M. Climatic, geomorphologic and hydrologic perturbations as drivers for mid- to late Holocene development of ice-wedge polygons in the western Canadian Arctic. *Permafr Periglac Process*. 2018;29(3):164-181. doi:10.1002/ppp.1977
17. Kowalewski DE, Marchant DR, Head JW, Jackson DW. A 2D model for characterising first-order variability in sublimation of buried glacier ice, Antarctica: assessing the influence of polygon troughs, desert pavements and shallow subsurface salts. *Permafr Periglac Process*. 2012;23(1):1-14. doi:10.1002/ppp.731
18. Lachenbruch AH. Mechanics of thermal contraction cracks and ice-wedge polygons in permafrost. *Geol Soc Am Spec Paper*. 1962;70:69. doi:10.1130/SPE70-p1
19. Plug LJ, Werner BT. Fracture networks in frozen ground. *J Geophys Res*. 2001;106(B5):8599-8613. doi:10.1029/2000JB900320
20. Mellon M, Mckay C, Heldmann J. Polygonal ground in the McMurdo Dry Valleys of Antarctica and its relationship to ice-table depth and the recent Antarctic climate history. *Antarct Sci*. 2014;26(4):413-426. doi:10.1017/S0954102013000710
21. Haltigin TW, Pollard WH, Dutilleul P, Osinski GR. Geometric evolution of polygonal terrain networks in the Canadian High Arctic: Evidence of increasing regularity over time. *Permafr Periglac Process*. 2012;23(3):178-186. doi:10.1002/ppp.1741
22. Ulrich M, Hauber E, Herzschuh U, Härtel S, Schirrmeister L. Polygon pattern geomorphometry on Svalbard (Norway) and western Utopia Planitia (Mars) using high-resolution stereo remote-sensing data. *Geomorphology*. 2011;134(3):197-216. doi:10.1016/j.geomorph.2011.07.002
23. Skurikhin AN, Gangodagamage C, Rowland JC, Wilson CJ. Arctic tundra ice wedge landscape characterization by active contours without edges and structural analysis using high-resolution satellite imagery. *Remote Sens Lett*. 2013;4(11):1077-1086. doi:10.1080/2150704X.2013.840404
24. Ulrich M, Grosse G, Strauss J, Schirrmeister L. Quantifying wedge-ice volumes in Yedoma and thermokarst basin deposits. *Permafr Periglac Process*. 2014;25(3):151-161. doi:10.1002/ppp.1810
25. Witharana C, Bhuiyan MAE, Liljedahl AK, et al. An object-based approach for mapping tundra ice-wedge polygon troughs from very high spatial resolution optical satellite imagery. *Remote Sens (Basel)*. 2021;13(4):558-579. doi:10.3390/rs13040558.
26. Zhang W, Witharana C, Liljedahl AK, Kanevskiy M. Deep Convolutional Neural Networks for Automated Characterization of Arctic Ice-Wedge Polygons in Very High Spatial Resolution Aerial Imagery. *Remote Sens (Basel)*. 2018;10(9):1487-1517. doi:10.3390/rs10091487
27. Brooker LM, Balme MR, Conway SJ, et al. Clastic polygonal networks around Lyot crater, Mars: Possible formation mechanisms from morphometric analysis. *Icarus*. 2018;302:386-406. doi:10.1016/j.icarus.2017.11.022

28. Marchant D, Head J. Geologic analogies between the surface of Mars and the McMurdo Dry Valleys: Microclimate-related geomorphic features and evidence for climate change. In: Doran P, Lyons W, McKnight D, eds. *Life in Antarctic Deserts and other Cold Dry Environments: Astrobiological Analogs*. Cambridge: Cambridge University Press; 2010:9-77. doi:10.1017/CBO9780511712258.002.

29. Sasseroth C, Hauber E, de Vera JP, Schmitz N. Quantitative Investigations of Polygonal Patterned Ground in Continental Antarctica: A Mars analogue. Proceedings: *European Planetary Science Congress* 2017, EPSC2017;11:839.

30. Fukuda M, Strelin JA, Shimokawa K, Takahashi N, Sone T, Trombotto D. Permafrost occurrence of Seymour Island and James Ross Island, Antarctic Peninsula region. In: Yoshida Y, Kaminuma K, Shiraishi K, eds. *Recent progress in Antarctic earth sciences*. Tokyo: Terra Scientific Publishing Co; 1992:745-750.

31. Matsuoka N, Hirakawa K. High-centered polygons in the Sor-Rondane Mountains, East Antarctica; possible effect of ice wedge sublimation. *Polar Geosci*. 2006;19:189-201.

32. Doolittle JA, Hardisky MA, Gross MF. A ground-penetrating radar study of active layer thicknesses in areas of moist sedge and wet sedge tundra near Bethel, Alaska. U.S.A. *Arctic Alpine res*. 1990;22(2): 175-182. doi:10.2307/1551302

33. Hinkel KM, Doolittle JA, Bockheim JG, et al. Detection of subsurface permafrost features with ground-penetrating radar, Barrow, Alaska. *Permafr Periglac Process*. 2001;12(2):179-190. doi:10.1002/ppp.369

34. Moorman BJ, Robinson SD, Burgess MM. Imaging periglacial conditions with ground-penetrating radar. *Permafr Periglac Process*. 2003; 14(4):319-329. doi:10.1002/ppp.463

35. Bode J, Moorman B, Stevens C, Solomon S. Estimation of Ice Wedge Volume in the Big Lake Area, Mackenzie Delta, NWT, Canada. Proceedings: *9th International Conference on Permafrost*. 2008:131-136.

36. Munroe JS, Doolittle JA, Kanevskiy MZ, et al. Application of ground penetrating radar imagery for three-dimensional visualisation of near surface structures in ice-rich permafrost, Barrow, Alaska. *Permafr Periglac Process*. 2007;18(4):309-321. doi:10.1002/ppp.594

37. Schennen S, Tronicke J, Wetterich S, Allroggen N, Schwamborn G, Schirrmeister L. 3D ground-penetrating radar imaging of ice complex deposits in northern East Siberia. *Geophysics*. 2016;81(1): WA195-WA202. doi:10.1190/geo2015-0129.1

38. Doolittle JA, Nelson F. Characterising relict cryogenic macrostructures in mid-latitude areas of the USA with three-dimensional ground-penetrating radar. *Permafr Periglac Process*. 2009;20(3): 257-268. doi:10.1002/ppp.644

39. Watanabe T, Matsuoka N, Christiansen HH. Ice- and Soil-Wedge Dynamics in the Kapp Linné Area, Svalbard, Investigated by Two- and Three-Dimensional GPR and Ground Thermal and Acceleration Regimes. *Permafr Periglac Process*. 2013;24(1):39-55. doi:10.1002/ppp.1767

40. Andres CN, Osinski GR, Godin E, Kukko A. The utility of 3D Ground-Penetrating Radar imaging to quantify subsurface ice volume: considerations for polygonal terrain network development. In: *Proceedings, 51st Lunar and Planetary Science Conference*; March 16-20. Texas, US: The Woodlands; 2020.

41. Yoshikawa K, Romanovsky V, Duxbury N, Brown J, Tsapin A. The use of geophysical methods to discriminate between brine layers and fresh-water taliks in permafrost regions. *J Glaciol Geocryol*. 2004;26: 301-309.

42. Dafflon B, Hubbard S, Ulrich C, et al. Geophysical estimation of shallow permafrost distribution and properties in an ice-wedge polygon-dominated Arctic tundra region. *Geophysics*. 2016;81(1): WA247-WA263. doi:10.1190/geo2015-0175.1

43. Watanabe T, Matsuoka N, Christiansen HH. Mudboil and ice-wedge dynamics investigated by electrical resistivity tomography, ground temperatures and surface movements in Svalbard. *Geogr Ann* 2012;

94(4): 445-457. https://www.jstor.org/stable/23360731. 10.1111/j.1468-0459.2012.00470.x

44. Léger E, Dafflon B, Soom F, Peterson J, Ulrich C, Hubbard S. Quantification of Arctic Soil and Permafrost Properties Using Ground-Penetrating Radar and Electrical Resistivity Tomography Datasets. *IEEE J Sel Top Appl Earth Obs Remote Sens*. 2017;10(10):4348-4359. doi:10.1109/JSTARS.2017.2694447

45. Baroni C, Orombelli G. Glacial geology and geomorphology of Terra Nova Bay (Victoria Land Antarctica). *Mem Soc Geol Ital*. 1987;33:171-193.

46. Orombelli G. Le spiagge emerse oloceniche di Baia Terra Nova (Terra Vittoria, Antartide) Atti *Acc. Lincei, Rend*. 1988;8:403-416. in Italian.

47. Carmignani L, Ghezzo C, Gosso G, et al. *Geological Map of the Area between David and Mariner Glaciers, Victoria Land, Antarctica. Scale 1: 5,000,000*. Firenze, Italy: Programma Nazionale di Ricerche in Antartide (PNRA); 1988.

48. Baroni C, Orombelli G. Holocene raised beaches at Terra Nova Bay, Victoria Land, Antarctica. *Quatern Res*. 1991;36(2):157-177. doi:10.1016/0033-5894(91)90023-X

49. Guglielmin M, Biasini A, Smiraglia C. Buried ice landforms in the Northern Foothills (Northern Victoria Land, Antarctica). Some results from electrical soundings. *Geographis Ann*. 1997;79a(1-2):17-24. doi:10.1111/1468-0459.00003

50. French HM, Guglielmin M. Observations on the ice marginal, periglacial geomorphology of Terra Nova Bay, Northern Victoria Land, Antarctica. *Permafr Periglac Process*. 1999;10(4):331-347. doi:10.1002/(SICI)1099-1530(199910/12)10:4.3.0.CO;2-A

51. Cannone N, Guglielmin M, Malfasi F, Hubberten HW, Wagner D. Rapid soil and vegetation changes at regional scale in continental Antarctica. *Geoderma*. 2021;394:115017. doi:10.1016/j.geoderma.2021.115017

52. Bromwich DH, Nicolas JP, Monaghan AJ. An assessment of precipitation changes over Antarctica and the Southern Ocean since 1989 in contemporary global reanalyses. *J Climate*. 2011;24(16):4189-4209. doi:10.1175/2011JCLI4074.1

53. Zhao W, Forte E, Colucci RR, Pipan M. High-resolution glacier imaging and characterization by means of GPR attribute analysis. *Geophys J Int*. 2016;206(2):1366-1374. doi:10.1093/gji/ggw208

54. Loke MH, Chamber JE, Rucker DF, Kuras O, Wilkinson PB. Recent development in the direct-current geoelectrical imaging method. *J Appl Geophys*. 2013;95:135-156. doi:10.1016/j.jappgeo.2013.02.017

55. Guglielmin M, Ponti S, Forte E. The origins of Antarctic Rock glaciers: periglacial or glacial features? *Earth Surf Process Landf*. 2018;43(7): 1390-1402. doi:10.1002/esp.4320

56. Cannone N, Guglielmin M. Relationships between periglacial features and vegetation development in Victoria Land, continental Antarctica. *Antarct Sci*. 2010;22(SI6):703-713. doi:10.1017/S0954102010000751

57. Guglielmin M, Dalle Fratte M, Cannone N. Permafrost warming and vegetation changes in continental Antarctica. *Environ Res Lett*. 2014; 9(4):045001. doi:10.1088/1748-9326/9/4/045001

58. Jol HM. *Ground Penetrating Radar: Theory and Applications*. Amsterdam, The Netherlands: Elsevier Science Ltd; 2009;524

59. Fortier D, Allard M. Late Holocene syngenetic ice-wedge polygons development, Bylot Island, Canadian Arctic Archipelago. *Can J Earth Sci*. 2004;41(8):997-1012. doi:10.1139/E04-031

60. Gamon JA, Kershaw GP, Williamson S, Hik DS. Microtopographic patterns in an arctic Baydjarakh field: do fine-grain patterns enforce landscape stability? *Environ Res Lett*. 2012;7(1):015502. doi:10.1088/1748-9326/7/1/015502

61. Fong T, Bualat M, Deans MC, et al. Robotic Follow-up for Human Exploration, proc. of *AIAA Space 2010 Conference and Exposition*, AIAA 2010–8605 American Institute of Aeronautics and Astronautics 30 August 2010–02 September 2010, Anaheim, California, US. 2010. doi:10.2514/6.2010-8605

62. Spate AP, Burgess JS, Shevlin J. Rates of rock surface lowering, Princess Elizabeth Land, Eastern Antarctica. *Earth Surf Process Landf*. 1995;20(6):567-573. doi:10.1002/esp.3290200608

63. Carracedo A, Rodés Á, Smellie JL, Stuart FM. Episodic erosion in West Antarctica inferred from cosmogenic 3He and 10Be in olivine from Mount Hampton. *Geomorphology*. 2019;327:438-445. doi:10.1016/j.geomorph.2018.11.019

64. Morgan DJ, Putkonen J, Balco G, Stone J. Degradation of glacial deposits quantified with cosmogenic nuclides, Quartermain Mountains, Antarctica. *Earth Surf Process Landf*. 2011;36(2):217-228. doi:10.1002/esp.2039

65. Gardner N, Hall B, Wehmiller J. Pre-Holocene raised beaches at Cape Ross, Southern Victoria Land, Antarctica. *Mar Geol*. 2006;229(3-4):273-284. doi:10.1016/j.margeo.2006.01.006

66. Raffi R. Ice wedges in the Terra Nova Bay region (Victoria Land, Antarctica): distribution and morphological features. *Terra Antartica Rep*. 2003;8:143-148.

67. Schennen SS, Bricheva SS, Tronicke JT. Potential of Ground-penetrating Radar for imaging active layer and ice wedges in permafrost areas. Proceedings: *Near Surface conference and exhibition*, 3–7 September 2017. Malmö, Sweden. doi:10.3997/2214-4609.201700399

68. Sokolov K, Fedorova L, Fedorov M. Prospecting and Evaluation of Underground Massive Ice by Ground-Penetrating Radar. *Geosciences*. 2020;10(7):274-287. doi:10.3390/geosciences10070274

SUPPORTING INFORMATION

Additional supporting information may be found in the online version of the article at the publisher's website.